Mon. Not. R. Astron. Soc. **000**, 1–16 (1998) Printed 1 February 2008 (MN LATEX style file v1.4)

Measurement of Star-Formation Rate from Hα in field galaxies at z=1

Karl Glazebrook,[1] Chris Blake,[2] Frossie Economou,[3] Simon Lilly,[4] Matthew Colless[5]
[1] *Anglo-Australian Observatory, PO Box 296, Epping, NSW 2121, AUSTRALIA*
[2] *Magdalen College, Oxford, OX1 4AU, UK*
[3] *Joint Astronomy Centre, 660 North A'ohoku Place, University Park, Hilo, HI 96720, USA*
[4] *Department of Astronomy, University of Toronto, 60 St George Street, Toronto, Ontario, M5S 3H8, Canada*
[5] *Research School of Astronomy & Astrophysics, The Australian National University, Weston Creek, ACT 2611, Australia*

arXiv:astro-ph/9808276v2 10 Feb 1999

1 February 2008

ABSTRACT

We report the results of J-band infrared spectroscopy of a sample of 13 $z = 1$ field galaxies drawn from the Canada-France Redshift Survey, targeting galaxies whose redshifts place the rest frame Hα line emission from HII regions in between the bright night sky OH lines. As a result we detect emission down to a flux limit of $\simeq 10^{-16}$ ergs cm^{-2} s^{-1} corresponding to a luminosity limit of $\simeq 10^{41}$ ergs at this redshift for a $H_0 =$ 50 km s^{-1} Mpc,$^{-1}$ $q_0 = 0.5$ cosmology. From these luminosities we derive estimates of the star-formation rates in these galaxies which are independent of previous estimates based upon their rest-frame ultraviolet (2800Å) luminosity. The mean star-formation rate at $z = 1$, from this sample, is found to be at least three times as high as the ultraviolet estimates. The dust extinction in these galaxies is inferred to be moderate, for standard extinction laws, with a typical $A_V = 0.5$–1.0 mags, comparable to local field galaxies. This suggests that the bulk of star-formation is not heavily obscured, unless one uses greyer extinction laws.

Star-forming galaxies have the bluest colours and a preponderance of disturbed/interacting morphologies. We also investigate the effects of particular star-formation histories, in particular the role of bursts vs continuous star-formation in changing the detailed distribution of UV to Hα emission. Generally we find that models dominated by short, overlapping, bursts at typically 0.2 Gyr intervals provide a better model for the data than a constant rate of star-formation. The star-formation history of the Universe from Balmer lines is compiled and found to be typically 2–3$\times$ higher than that inferred from the UV *at all redshifts*. It can not yet be clearly established whether the star-formation rate falls off or remains constant at high-redshift.

Key words: surveys – cosmology: observations – galaxies: evolution – galaxies: starburst – stars: formation

1 INTRODUCTION

The topic of the history of star-formation in the Universe has excited much interest in recent years, stimulated by the first observations of nearly-normal star-forming galaxies at $z > 3$ (Steidel *et al.* 1996). Previously high-redshift studies were limited to highly active galaxies that may be poor tracers of the typical star-formation history of the universe as a whole. Steidel *et al.* used the colour signature of the Lyman break/Lyman-α forest discontinuity being redshifted through optical filters to select high-redshift objects (Guhathakurta *et al.* 1990), these were subsequently confirmed spectroscopically on the 10m W.M. Keck telescope.

Comparison of these objects with the low-redshift ($z < 1$) samples of field galaxies (Lilly *et al.* 1995, Ellis *et al.*, 1996) appears to show a rise in the Universal star-formation rate from $z = 0$ to $z = 1$ and a drop-off at $z > 3$ indicating a star-formation peak in the $z = 1$–2 epoch (Madau *et al.* 1996). This is also inferred to be the epoch when large galaxies with classical elliptical and spiral morphologies are assembled: Hubble Space Telescope observations indicate they are extant at $z = 1$ (Brinchmann *et al.* 1998, Lilly *et al.* 1998) but absent in the $z > 3$ sample (Giavalisco *et al.* 1996, Lowenthal *et al.* 1997). Theoretical developments using galaxy formation simulations constrained by the ob-

© 1998 RAS

served evolution in the density of neutral gas from Lyman-α QSO absorbers show qualitative agreement with this picture (Fall *et al.* 1996).

However these measurements of star-formation rate are based upon the measurement of ultraviolet continuum luminosity, 1500–2800Å in the rest-frame, assumed to be from young stellar populations. If dust extinction played a significant role in obscuring UV radiation they could be underestimated by large factors which may change the picture completely.

A more robust way to measure the star-formation rate of high-redshift galaxies would be to measure their luminosities in Balmer recombination lines. This radiation come from reprocessed ionising radiation emitted by young stars. This approach has two advantages: firstly the ionising radiation comes from more massive short lived stars than the softer 1500–2800Å UV and hence falls quickly to zero only 20 Myr after star-formation stops. Thus the Balmer luminosity is a more direct measure of the *instantaneous* star-formation rate. This contrasts with the UV which continues to rise as the stellar populations evolve, typically doubling for example between 10 and 1000 Myr at 1500Å. For Hα the main dependence is directly on the Initial Mass Function and negligibly on the temporal evolution.

The second main advantage is that the Balmer radiation is emitted in the red part of the optical spectrum and is thus much less affected by any dust extinction or attenuation than the ultraviolet. For example for typical SMC and Milky Way extinction laws (Pei 1992) the 1500Å and 2800Å extinctions (in magnitudes) range from 2–7 times greater than that at Hα (6563Å).

However to observe Hα at high-redshift requires infrared spectroscopy, which has not been possible until recently because of the faintness of the sources involved. Pettini *et al.* (1998) have secured the first IR spectra of 5 of the $z > 3$ Steidel *et al.* galaxies, and obtained Hβ luminosities. In this paper we report the results of the first measurements of the Hα line in a sample of normal $z \simeq 1$ field galaxies drawn from the Canada-France Redshift Survey (Lilly *et al.* 1995, Le Fevre *et al.* 1995, Lilly *et al.* 1995B, Hammer *et al.* 1995). This sample (hereafter 'CFRS') is a highly-complete redshift survey of a magnitude-selected ($I_{AB} < 22.5$) sample of normal field galaxies. The median redshift is 0.6, and galaxies extend out to $z = 1.3$. Because the sample is magnitude selected the $z \gtrsim 1$ end is dominated by luminous $L \sim L^*$ galaxies.

2 OBSERVATIONS AND DATA REDUCTION

The observations were carried out on May 10-11 and October 3-5 1996 at the UK Infrared Telescope in Hawaii using the CGS4 spectrograph (Wright 1994). We chose galaxies in the redshift range 0.790-1.048 so that the Hα line would lie in the relatively clean part of the near-infrared J-band (1.17-1.34 μm) where the atmospheric extinction is relatively low ($< 15\%$). We also selected galaxies with detectable [OII] emission in the optical CFRS spectra which make up 85% of the CFRS sample at $z \sim 1$.

As well as absorption, the J-band is contaminated by numerous airglow OH emission lines, which increase the broad-band sky-brightness by a factor of 30 and hinders the detection of faint objects. Our observational strategy was to observe at high-resolution with CGS4, thus resolving out the OH background. Because we already knew the galaxies' redshifts from the optical spectra the limited wavelength coverage at high-resolution was not a problem. Moreover we could exclude galaxies whose redshifts would put the Hα line on or close to an OH line. (A similar strategy was also adopted by Pettini *et al.*) We observed with the 150 lines/mm grating and the 1 arcsec/1 pixel slit giving a resolution $\lambda/\Delta\lambda = 2200$. We determined empirically that at this resolution OH lines contaminated 50% of the bandpass, *i.e.* we had to exclude 50% of the high-redshift galaxies, but in the remaining clean part of the bandpass the mean background was only 20% that of broad J.

Targets were acquired using the following procedure: first we 'peaked-up' on a very bright star ($V = 1 - 2$ mags) within 1–2 degrees of the target. This involves centering the star on the optical finder TV, reading the IR array in a continuous 'MOVIE' mode, and then adjusting the offset between the axis of CGS4 and the TV until the IR flux is maximised. This assures the IR slit is aligned with the TV crosshair. Then we went to a fainter star, typically 17th mag, within 1–2 arcmin of our target galaxy and measured off the same coordinate system, centered the star on the TV crosshair and did a blind offset on to the target galaxy. (The targets were too faint to see on the TV). We would then autoguide either on the offset star or another bright star in the region.

Observations were made stepping the InSb detector array in 0.5 pixel increments to fully sample the instrument profile and nodding the telescope $\pm$ 9 arcsec along the slit between 'OBJECT' and 'SKY' positions to facilitate sky-subtraction (though note the object is still on the slit in both positions). Individual exposures ranged from 10-15 minutes. The typical seeing was 1.0 arcsec. A total of 13 objects were observed: these are listed with their total exposure times in Table 1. Standard wavelength calibration and flatfield corrections were applied. The October observing run was affected by the spectrograph slit being jammed out of position which caused the lines to be tilted on the image. The shifts were measured by cross-correlation and the tilt corrected by re-interpolation.

Even with the resolved OH background accurate sky-subtraction is critical to detection of faint lines. To first order the sky can be removed by simply subtracted the pairs of offset frames, though this leaves residual signal due to temporal sky changes. To second order the residual sky was removed by performing a polynomial interpolation along the slit, excluding the two object regions, and subtracting. This leaves no systematic residual, though the regions near the OH lines are still noisier due to the extra Poisson contribution, with the result being a 2D image with a positive spectrum in the 'OBJECT' row and a negative spectrum in the 'SKY' row. For each image we also made a pixel mask to exclude bad pixels on the detector and regions with noisy OH residuals.

In many of the images there were strong Hα and continuum detections. We summed all the Hα lines with good detections, fitted Gaussians spectrally and spatially to define the typical line profile and then used this mean profile (with the pixel mask) to optimally extract all bright, faint and possibly non-detected objects in a consistent manner.

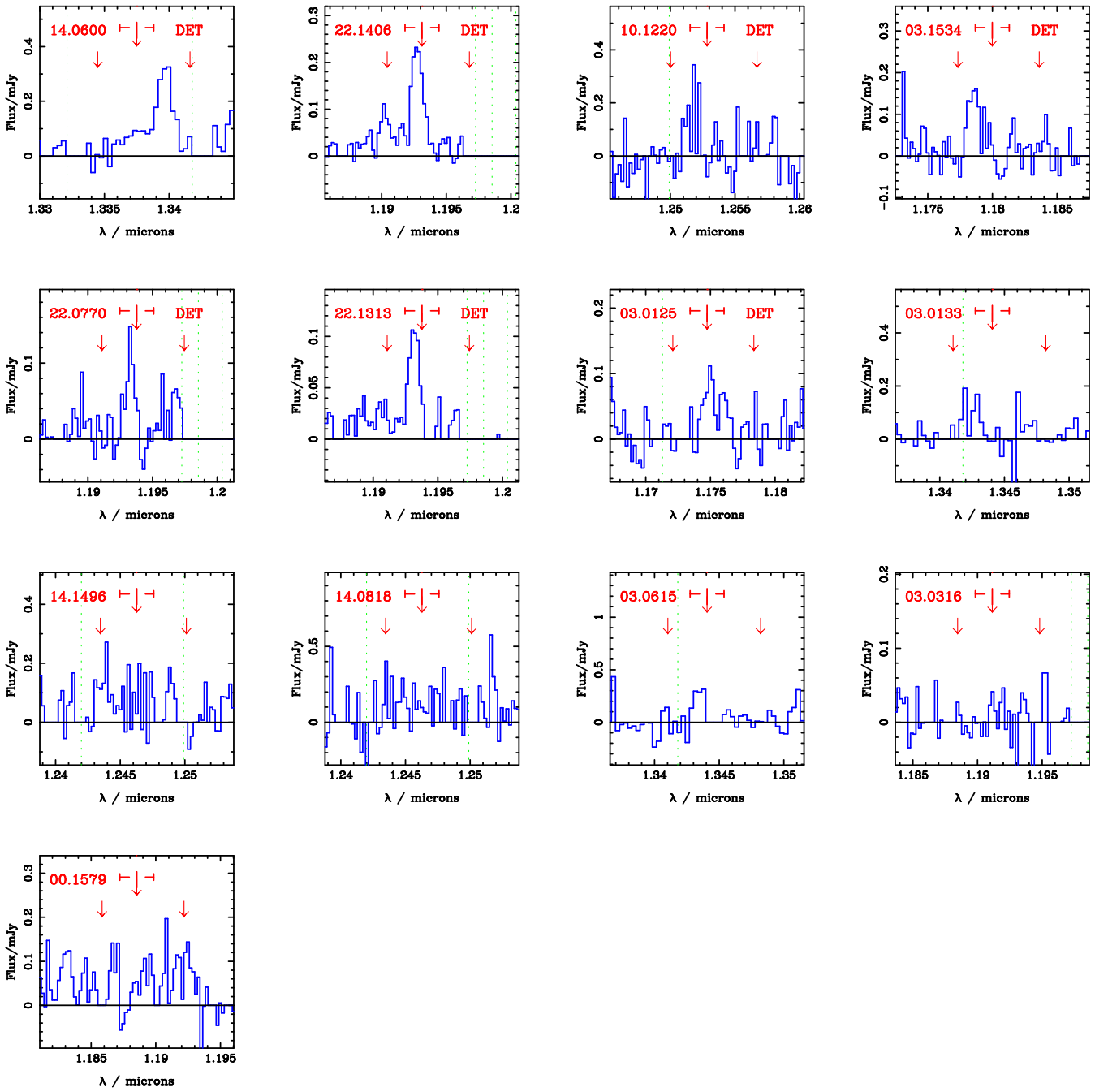

Figure 1. The J-band spectra of our CFRS galaxies. The spectra have been continuum subtracted and centered on the Hα line. The large central arrow indicates the predicted Hα position based on the optical redshift, the associated horizontal error bar denoting the 1σ error on the redshift. The two smaller arrows show the predicted positions of the [NII] 6548Å and 6583Å lines. The vertical dotted lines indicate the positions of strong night sky OH lines which have been masked out. The objects where we find a $> 2\sigma$ Hα detection are labelled 'DET.'

In most of our observations we found that the negative spectrum was typically weaker, or even absent, compared to the positive spectrum. This is attributed to the fact that any small errors in acquisition are magnified when stepping 9 arcsec away from the centre along the slit as the rotation is not precisely known. When there was a significant negative spectrum it was combined in a weighted manner (to maintain consistent exposure times) into the positive spectrum. This marginally increases the signal/noise, though none of the flux measurements presented below are significantly changed if this step is omitted.

Next the spectra had atmospheric absorption removed using a smooth-spectrum standard and were flux calibrated using flux standards.

Finally we applied aperture corrections to allow for our finite 1.0 arcsec wide slit. Our objects are resolved, our mean Gaussian spatial profile along the slit of the Hα line has a FWHM of 2.0 arcsec (which is consistent with the typical 3–

5 arcsec isophotal optical diameters measured for the CFRS sample (Hammer *et al.* 1997)). The flux calibration stars are observed through the same slit in 1.0 arcsec seeing. Assuming Gaussian profiles for both we derive a relative correction factor of 1.7, by which we multiply our spectra. While this can only be a rough correction, it gives fluxes consistent with the optical lines (see section 3). It is also only of order unity, so even if ignored our conclusions below are not drastically altered.

The continuum level was determined in each case by taking the mean of the data points ± 0.02 microns either side of the emission line, ignoring the masked points and the emission line. The noise level of the data was determined empirically from the RMS in the same region. In most cases we found significant continuum emission. Note that for individual pixels the continuum is mostly below the noise, it is only by summing up we get a significant detection. To check the validity of our measurements we repeated the same procedure for an off-object row in the longslit spectra. This give non-detections in all cases, so we are confident in our procedure.

After subtraction of the continuum level from the data we computed the line flux by summing the flux $\pm N$ pixels around the line, excluding the masked pixels, where $N = 7$ is chosen to be the typical line FWHM. This is done regardless of whether there appears to be a detection or not (as the expected wavelength is known).

The final line fluxes and continuum fluxes (converted to AB mags and denoted J_C) are given in Table 1, along with the most useful CFRS parameters of our objects. Hα fluxes $< 1\sigma$ are set $= 0$. We find 7 detections $> 2\sigma$ and 5 detections $> 3\sigma$ out of our 13 objects.

We convert these to luminosities using a $H_0 = 50$ km s^{-1} Mpc,$^{-1}$ and $q_0 = 0.5$ cosmology in Table 2. We use this cosmology for the rest of our paper. We note that in our further analysis our conclusions are based on comparing the luminosities of the same galaxies at different wavelengths, since all the galaxies in our sample lie close to $z = 1$ our conclusions are essentially unchanged if we use a different cosmology.

To complete the quantities derived from the lines we fit Gaussians profiles (excluding masked pixels) to derive velocity line widths for all our detections. Each of the fits was checked visually by plotting on top of the line; the instrumental resolution was determined by fitting to unresolved night-sky OH lines in the region of the galaxy line and the value was subtracted in quadrature from the galaxy line widths. It should be noted that all our lines, but one, are well-resolved as we expected given the spectral resolution and the typical velocity widths of galaxies. The spectra line Full Width Half Maximum (FWHM) of the galaxies range from 3–5 pixels (one pixel = 2–3 Å depending on the spectrum) compared to 2.4–2.6 pixels for the sky lines. The results are presented in Table 2; we make no detailed analysis here, we just note that the typical velocity FHWMs are in the range 200–400 km/sec expected for large $L \sim L_*$ galaxies.

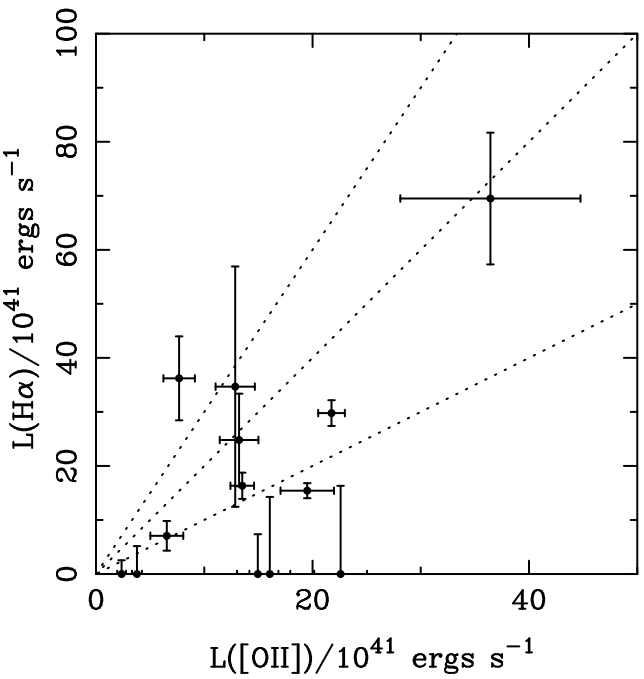

Figure 2. Comparison of line luminosities of the sample in [OII] and Hα. Dotted lines show slopes of Hα/[OII] $= 1, 2, 3$, the spread of ratios found be Kennicutt (1992).

3 COMPLETENESS

In 8/13 of the galaxy spectra Hα emission was detected; additionally 9/13 of the galaxies had detected continuum emission. This proves quite useful: we can check if our line non-detections are due to poor acquisition by comparing the continuum level of our line detections and non-detections. There are only two cases in which there is no line *and* no continuum detection. The general trend is that the average continuum flux is *brighter* for the non-detections, this translates in to an median $(I-J_C)_{AB}$ colour 1.1 mags *redder*. This argues against the slit missing the object, in fact the trend towards redder colours is precisely what is expected for non-line emitting objects. We note that at $z = 1$ a Scd galaxy should have observed colours $(I - J)_{AB} = 1.0$ and an E/SO galaxy $(I - J)_{AB} = 2.0$, using template SEDs from Kennicutt (1992). We find median colours of $(I - J)_{AB} = 1.6$ for the Hα detections and $(I - J)_{AB} = 2.7$ for the non-detections, which agree very well given our actual galaxies will differ in detail from Kennicutt's templates.

Figure 1 shows the final set of spectra, which have been continuum subtracted and centered on the Hα line. The line is in all cases found within the error box given by the optical redshift ($\Delta z \simeq 0.002$). Our resolution is high enough that Hα is well separated from the [NII] lines so we do not have to correct for blending. Also in a few cases (e.g objects 22.1406 and 22.070) we see evidence for one of the weaker [NII] lines as well as the main Hα line. This is additional evidence for the robustness of our detections. Note in many cases the position of one or both of the [NII] lines is occluded by a noisy OH residual.

We can also test our completeness using CFRS values for the [OII] flux (Hammer *et al.* 1997) to calculate a Hα/[OII] line ratio. In the CFRS sample in this redshift

range 85% of galaxies have [OII] emission. Hammer *et al.* tabulate the [OII] equivalent width and flux, the latter is aperture-corrected by comparing the spectra at $\sim$ 5500Å with their V-band image photometry. Other than excluding galaxies with zero [OII] emission we made no attempt to concentrate on objects with the strongest [OII] emission. Thus the mean [OII] equivalent width (32Å) and range (10–60Å) of our small sub-sample are consistent with random sampling from the larger sample. The CFRS galaxies at $z = 1$ with zero [OII] are all at the red end of the colour distributions in $V - I$ and $I - K$. Thus the colours also indicate they are not significant star-forming systems and we conclude their exclusion has no significant impact on our conclusions below.

One might also ask the question: is the lack of Hα detection in some of our objects consistent with the *presence* of [OII] in our optical spectra? This is addressed in Figure 2 where we plot the strength of the two lines against each other. It can be seen that given the Hα error bars all points are consistent with a reasonable linear correlation. Kennicutt (1992) estimates the line ratio Hα/[OII] as having a median value of about 2 (with a spread from 1 to 3) for a sample of local star-forming galaxies (1.0 mag mean extinction). Our observed values at high-redshift are entirely consistent with Kennicutt's median and spread, implying we too have small amounts of extinction which agrees with our findings below in Section 5. The points with zero Hα are consistent with detected [OII] given the larger error bars. Note the line ratios are also good evidence that our aperture corrections are reasonable, if omitted we would obtain a much lower ratio Hα/[OII] = 1.

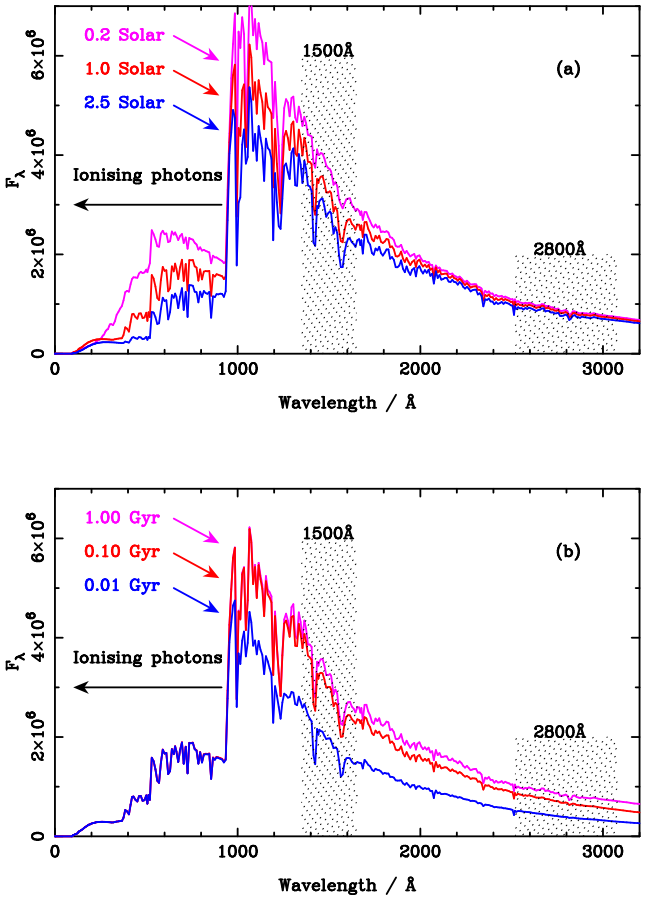

Figure 3. Illustration of the dependence of the UV spectrum on metallicity and time for a constant star-formation rate. These are theoretical galaxy spectra from the BC96 population synthesis models (Salpeter IMF). The position of the 1500Å and 2800Å ±10% bands are marked along with the ionising photons which are reprocessed into Hα. The vertical order of the labels is the same as the vertical order of the spectra. Panel (a) shows the spectrum at 1 Gyr for a decreasing metallicity sequence. Panel (b) shows the solar metallicity spectrum for an increasing time sequence. It is easily seen that while the redder UV bands are relatively insensitive to metallicity they are strongly time dependent until 1 Gyr old. The reverse is true for the ionising photons — the stellar spectra below 912Å are identical for times > 20 Myr at a given metallicity. Hence the resulting Hα flux is mainly dependent on metallicty.

4 STAR FORMATION RATES FROM Hα AND UV

Using models of population synthesis it is possible to calculate the relation between input star-formation rates and output UV and Hα fluxes. The basic principle is that the UV light is dominated by short-lived main sequence stars (the Hα light is reprocessed ionising UV) so the number of them in a galaxy is proportional to the star-formation rate. The prescription for this calculation is simple. For reference we outline it (and the corresponding assumptions) in detail:

(i) For a given time-dependent star-formation rate the population synthesis code gives the UV stellar spectrum as a function of time. Note that Kennicutt (1983) in deriving his calibration uses a simple grid of stars of different masses with evolutionary tracks current at the time.

(ii) For the UV continuum estimators one takes an averaged flux (e.g. through a synthetic box filter) at a specific wavelength (e.g. 1500Å, 2800Å). At the longer wavelengths, with increasing stellar lifetimes, the conversion from a constant star-formation rate to a UV flux is age-dependent (see for example Pettini *et al.* who uses different factors at 1500Å for 10^7 and 10^9 years). One then also needs to apply corrections for dust attenuation and/or Lyman absorption by line of sight systems (e.g. Madau 1995).

(iii) For Hα one calculates the number of ionising Lyman continuum photons. This flux comes from the most short lived stars radiating at $\lambda < 912$Å with lifetimes of $\lesssim 10$ Myr. Then it is assumed all this radiation is absorbed by intervening hydrogen gas in the galaxy in which the forming stars are embedded and that none leaks out. In practice it seems this is very close to the truth. At very high-redshift the Lyman limit can be observed in the optical (e.g. the Steidel *et al.* galaxies) and the flux does indeed go to zero, but as these galaxies are identified by the Lyman breaks this could be a selection effect. For local galaxies there have been limited $\lambda < 912$Å spectroscopy, for example Leitherer *et al.* (1995) observed a sample of 4 starburst galaxies with the Hopkins Ultraviolet Telescope and concluded that < 3% of the ionising photons escaped. Constrained models of the ionising radiation field of the Milky Way (Bland-Hawthorn & Maloney 1997, 1998) indicate that approximately 5% may escape.

(iv) The ionising photons are reprocessed into recombi-

nation lines, and the relative strengths can be calculated in detail. Hummer & Storey (1987) calculate 0.45 Hα photons are emitted per Lyman continuum photon for case B recombination. This number is quite robust, over a range of nebulosity conditions (10^2-10^6K, 10^2-10^4 electrons cm^{-3}).

As there are a number of values for these conversion factors in the literature we thought it would be useful for reference purposes to systematically tabulate these for a set of models. This also serves to illustrate the range of variations and trends. The results of our calculations are given in Table 3 for UV 1500Å, 2800Å and Hα conversions. The Bruzual & Charlot (1993, 1996) models ('BC96') offer a range of metallicities (albeit using theoretical model atmospheres — the 'kl96' models). The PEGASE models (Fioc *et al.* 1997) offer two sets of post-main sequence evolutionary tracks but only solar metallicity. Both sets of models offer several Stellar Initial Mass Functions (IMFs); we tabulate the results using the IMFs of Salpeter (1955) and Scalo (1986) because these bracket the upper and lower limits of the variation. We also tabulate some other values given previously in the literature.

For all these models Hα reaches a constant asymptote after 20 Myr, then stays constant to within a 5–10% out to 10 Gyr. Thus it can be used as a tracer of the instantaneous star-formation rate on time-scales of order ∼10 Myr. For reference we give the value at 100 Myr. The conversion is very sensitive to the IMF, as the ionising flux comes from the most massive stars, with Salpeter giving a value 2.8–3.4 × higher than Scalo for the different models. Another important point, which has not been remarked upon in the literature discussing high-z galaxies, is the strong effect of metallicity below 912Å. This occurs in the stellar evolutionary models because the most luminous stars (contributing below 912Å), have a much greater dependence of effective temperature on metallicity than the less luminous stars contributing at longer wavelengths. The effect of the hotter stars at low metallicty is to raise the Hα flux about 1.7 × compared to the solar metallicity value for a given star-formation rate.

The average UV luminosity per unit Hz is computed as the total energy integrated through a ± 10% box filter divided by the total bandwidth. This gives a negligible colour term. For a 10% filter the difference in the average between a constant f_ν spectrum (which approximates these spectra for $> 912\AA$) and a much redder constant f_λ spectrum is only 1%. The IMF dependence is somewhat less than for Hα (typically a factor of 1.5–2.5) as these UV bands come from less massive stars and the metallicity dependence on temperature is much smaller.

However there is a stronger time dependence, with the flux increasing significantly between 10^7 and 10^{10} years, especially at 2800Å and for the Scalo IMF which is much less rich in massive stars. For cosmological times (> 1 Gyr) the 1500Å flux is relatively insensitive to time as noted by Madau *et al.* (1998) (except for the extreme 0.02 Solar metallicity case). Thus it can be used as a tracer of the star-formation rate on time-scales of 1 Gyr. The 2800Å flux is not as stable and changes at the 10–40% level over 1–10 Gyr. There are further $\lesssim 50\%$ variations in the exact conversion depending on the model and metallicity assumed.

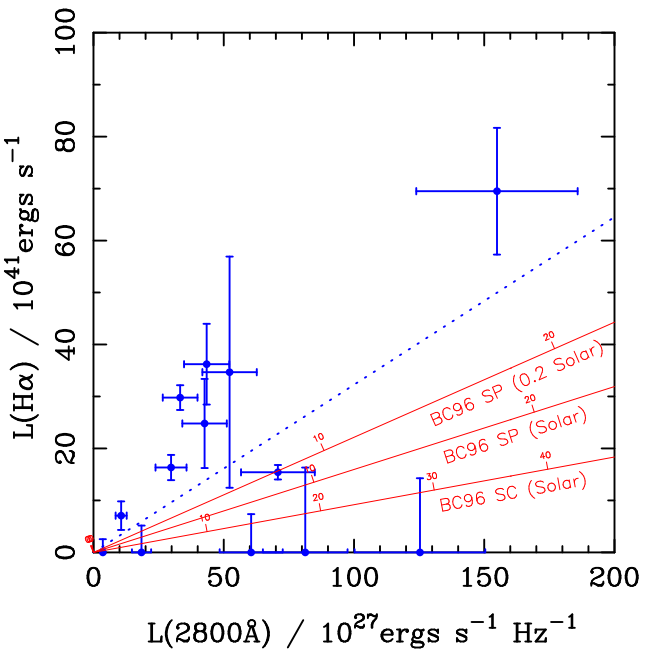

Figure 4. Comparison of the Hα vs UV continuum flux at 2800Å for the individual galaxies. The overlayed axes show the locus of constant star-formation rate for a set of fiducial models covering the range of UV/Hα ratios given in the last column of Table 3. The numeric labels on the axes are the corresponding star-formation rates in $M_\odot\,\mathrm{yr}^{-1}$. The dotted line shows the ratio of the mean luminosity densities derived in Section 5.

These time and metallicity effects are illustrated graphically in Figure 3. Finally it is worth noting that the range in the *ratio* of Hα to UV is less than the absolute range; as both come from high-mass stars the choice of IMF matters somewhat less.

5 THE STAR-FORMATION RATE AT $Z = 1$

Turning back to our data we can do a direct galaxy by galaxy comparison of the star-formation rates inferred from UV and Hα.

Our UV fluxes are particularly robust because for redshifts near unity the rest frame 2800Å light corresponds very closely to the observed frame V-band light. To a first approximation we can simply ignore the K-correction and derive the 2800Å flux directly from the CFRS V-magnitudes. We refine this slightly by using the SED fits from Lilly *et al.* (1996); this corrects the fluxes by 10–20%. Thus the UV luminosities we use are the same as the raw data which goes into the $z = 1$ star-formation rate determinations of Madau *et al.* (for $0.2 \leq z \leq 1$ this was based on the CFRS luminosity density functions of Lilly *et al.* 1996) We use a formal error bar of 20% for our UV fluxes to give errors representative of the V photometric errors and the K-corrections.

We plot the Hα vs UV luminosities in Figure 4 and overlay lines for a set of conversions from Table 3. Note these are only valid for a continuous, constant star-formation rate — the more complex problem of bursts is considered below in Section 6.

It is clear from the plot that there is a order-of-

magnitude agreement in the star-formation rates derived from the two methods and a reasonable correlation, i.e. strong UV systems are usually strong Hα systems. There are no galaxies with an extremely large excess of Hα relative to UV, which would occur if the star-formation was highly obscured by dust.

We do find points with zero Hα flux and appreciable UV flux, which we would expect to detect within the measurement errors if there was a linear correlation. This can not be due to dust as the latter can only enhance the UV/Hα ratio not diminish it. As noted in Section 3, these spectra are detected, they just do not contain significant Hα. One physical effect that will explain this is the relative lifetimes of stars contributing to the UV and Hα as mentioned in Section 4. When one moves away from the simple scenario of constant star-formation rate the picture changes considerably. For example for a instantaneous starburst the Hα flux will drop to effectively zero after 30 Myr while significant UV flux will persist up to 1000 Myr. This will produce low Hα points such as are seen in our sample. *Weak* Hα should be present in *all our galaxies* because they are known to have [OII] emission (see Section 3), however the UV/Hα ratio will scatter more widely and it is certainly possible for Hα to be below our detection limit despite significant [OII] and UV emission. To quantify these effects requires us to develop a proper model for starburst activity in galaxies. We do this below in Section 6.

Nevertheless when one averages over many galaxies the effect of bursts should cancel out in the mean — the continuous star-formation conversions of Table 3 should be applicable for an *ensemble* of galaxies. (This approximation is tested below using the methods developed in Section 6 and is found to accurate to $\sim \pm 10\%$, even for this small sample.) It can be seen that the values scatter about a ratio of 2–3 times as much star-formation inferred from the Hα as UV. This is balanced to some extent by the zero points. By summing over *all* the galaxies we find the following relation between the luminosity per comoving volume in Hα and UV:

$$\frac{L(2800\text{Å})}{\mathrm{L(H}\alpha)} = 3.1 \pm 0.4$$

in the units as in the last column of Table 3. This ratio is plotted as the dotted line in Figure 4.

The ratio is somewhat lower that those predicted by the models which give values in the range 4–14 for 0.2-2.5 Solar metallicities. What can cause this discrepancy? It is too large to be encompassed by our range of metallicities; one can boost the UV/Hα ratio if we assume a younger age than $\sim$ 1 Gyr. However changing to 0.1 Gyr only increases the slopes of the solid lines in Figure 4 by $\sim$ 30%; we could achieve the observed slope if star-formation is only $\sim$ 0.01 Gyr old in all the detected galaxies but this would be unlikely simply due to random sampling — the redshift range of the sample corresponds to a timespan of $\simeq$ 1 Gyr at $z = 1$. The most likely explanation for the discrepancy is the presence of dust attenuating the ultraviolet light.

If we adopt fiducial model values of (10.9, 6.3) for (Scalo, Salpeter) for Solar metallicity, which agree well between PEGASE and BC96 models (kl96 tracks), the ratio of Hα to UV inferred star-formation rates are (3.5, 2.0). Using Pei (1992) extinction formulae (a standard dust-screen model) we then derive a mean sample A_V of (1.0, 0.5) mags for the SMC law, (1.1,0.6) for the Galactic law.

These extinction values are entirely consistent with what is found from studies of star-formation from Balmer lines in local normal Sab galaxies. For example Kennicutt (1983) found $A_V = 1.0$ mags and a study of low redshift $z < 0.3$ CFRS galaxies using the $H\beta$/Hα line ratios by Tresse and Maddox (1998) found the same value.

Calzetti *et al.* (1994) and Calzetti (1997) have proposed an empirical dust-attenuation law for heavily reddened starbursts ($A_V \simeq 2.2$ mags). In this model the nebular lines have about twice the optical depth as the stellar continuum; moreover although the lines are well described by a standard Galactic screen law the stellar continuum is empirically described by a greyer law in which the dust and stars are intermixed. Using the Calzetti law we derive A_V attenuations of (2.6, 1.4) mags (for stars; ×1.4 for nebulae); because the attenutations of the Hα and 2800Å continuum are more similar than for the screen models a much higher obscuration is required to match the observed excesses: attenuations of (2.9, 1.6) mags result for Hα and (4.2, 2.3) mags for 2800Å stellar continuum. It should be noted however that it is still not established that corrections derived for the Balmer lines in starburst regions of nearby galaxies are appropriate to the integrated light of the distant galaxies studied here. This question remains open.

We can now examine the total correction for dust in both the Hα and UV determined star-formation rates. The Milky way law gives corrections for (Scalo, Salpeter) IMFs of $\times(2.2, 1.5)$ for Hα and (8.0,3.1) for the UV. These numbers are the same to within ±10% for the SMC extinction law; this is because the two extinction curves differ most strongly in the UV at $<<$ 2800Å (e.g. at the 2175Å dust feature) and in the near-UV and optical they are very similar. The Calzetti law of course gives much larger values: the final star-formation rates are an additional factor of $\sim 6\times$ higher for the Scalo IMF and $\sim 3\times$ higher for the Salpeter IMF.

Finally we can compare the star-formation rate of our $z \sim 1$ CFRS galaxies with local counterparts. We adopt the Salpeter IMF as that is conventionally used for deriving the local rates. For the range of dust corrections we have derived we obtain rates of $\sim$ 20–60 $M_\odot$ yr^{-1}, comparable to local starbursts (e.g. Calzetti 1997) and much greater than the typical 4 $M_\odot$ yr^{-1} found for local normal spirals (Kennicutt 1983) and the Milky Way (Smith *et al.* 1978).

6 MODELING OF STARBURSTS

As noted earlier the interpretation of Hα and UV luminosities as star-formation rates becomes more complicated if non-constant star-formation histories are assumed. For this reason we developed a mathematical frame-work for exploring this and to see how well we could reproduce the observed distribution.

6.1 Methods

The principles are based upon maximum likelihood and are a 2D generalisation of the methods developed by Abraham *et al.* 1999 for colour-colour fitting. For a given star-formation history we can run a spectral evolution code and

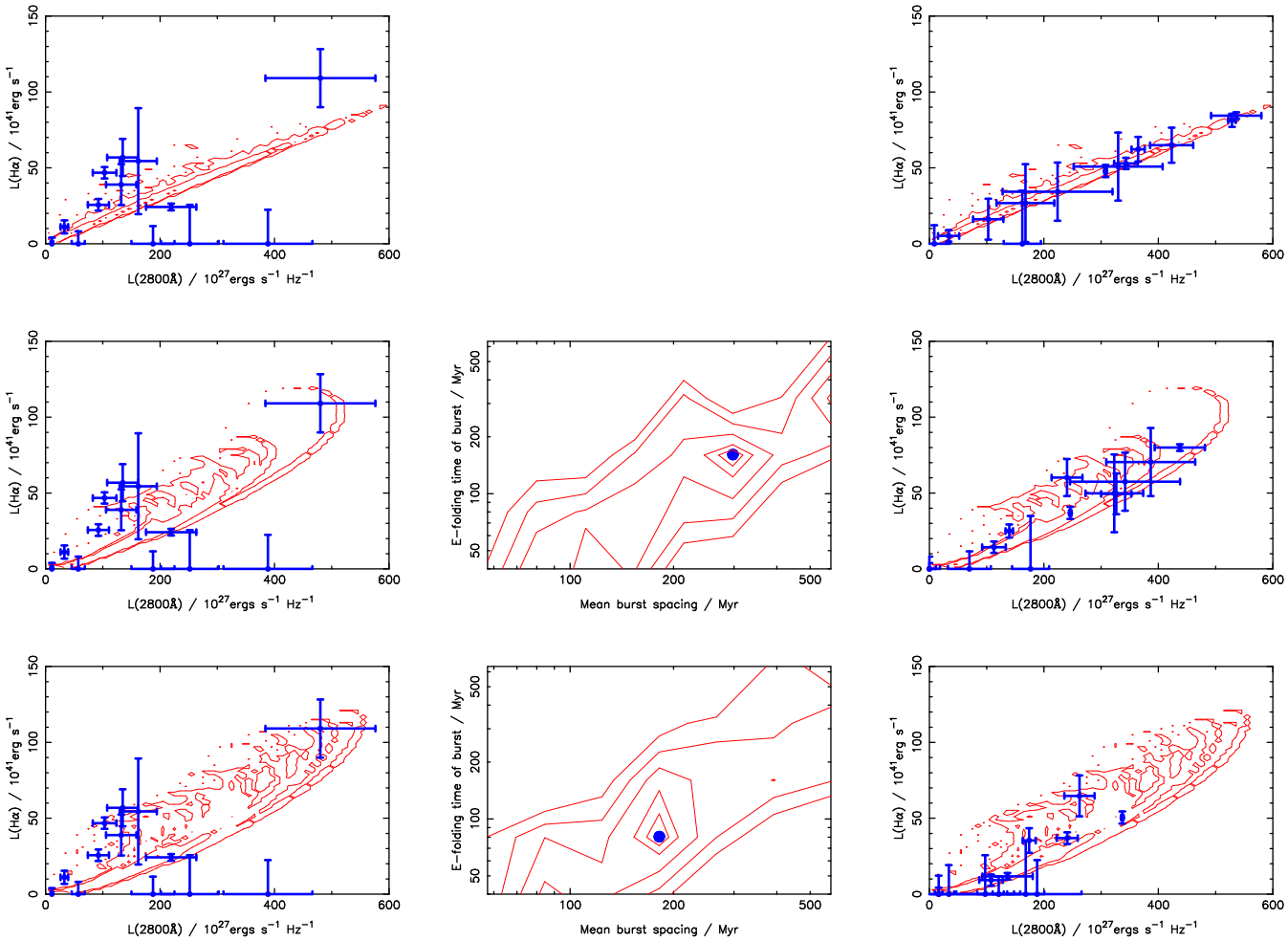

Figure 5. Results of fitting burst models to our extinction-corrected Hα and UV (2800Å) data. The three rows show three different models as described in the text, they are: continuous star-formation (top row), fixed mass exponential bursts plus continuous star-formation (middle row) and variable mass exponential bursts plus continuous star-formation (bottom row). The left hand column of panels shows the observational data (points) compared with a model distribution generated from the best fit model (contours correspond to a factor of 10 in probability density). The middle column of panels show the likelihood contours of the main burst parameters generated by our fitting. (Contours correspond to a factor of 10 in likelihood, the circle marks the maximum likelihood point.) The right hand column show a *realisation* of the best fit model, *i.e.* 13 simulated data points generated from the model distribution with the observed errors (points $< 1\sigma$ are set $= 0$ as in the data). Note the continuous star-formation includes a component of galaxy–galaxy scatter.

calculate Hα and UV luminosity as a function of time using the methods of Section 4. We evolve the models for 5 Gyr and sample at random times (we can do this because all the galaxies are at similar redshift) to create a 2D model distribution of light in the the (Hα, UV) plane. The code then computes the likelihood of drawing the observational data from the model:

$$\mathcal{L} = \prod_i \int_{-\infty}^{\infty}\int_{-\infty}^{\infty} \frac{P(h,u)\exp\left(-\frac{(h_i-h)^2}{2\Delta h_i^2} - \frac{(u_i-u)^2}{2\Delta u_i^2}\right) du\, dh}{2\pi\Delta h_i \Delta u_i}$$

where the observational (Hα, UV) points are (h_i, u_i) with errors $(\Delta h_i, \Delta u_i)$, and the model points have probability density $P(h,u)$.

The star-formation histories are parameterised and likelihood space is explored to find the maximum likelihood. We use an adaptive algorithm where a large parameter space is explored with a coarse parameter grid to locate the peak and the region around the peak is then examined with a finer grid to give confidence limits on the fitted parameters from $\Delta\mathcal{L}$.

Once we have the best fit parameters for a model, we can then create simulated observational datasets. This is done 1000 times, the maximum likelihood fit being recomputed each time, this allows us to normalise our relative likelihood into an absolute probability of the observed data given the model.

6.2 Star-formation histories explored

We parameterised the star-formation histories as continuous star-formation, with galaxy to galaxy scatter, plus a random distribution of bursts. Initially the total star-formation rate is kept constant and normalised to the values derived in Section 5. This is a good approximation as an ensemble

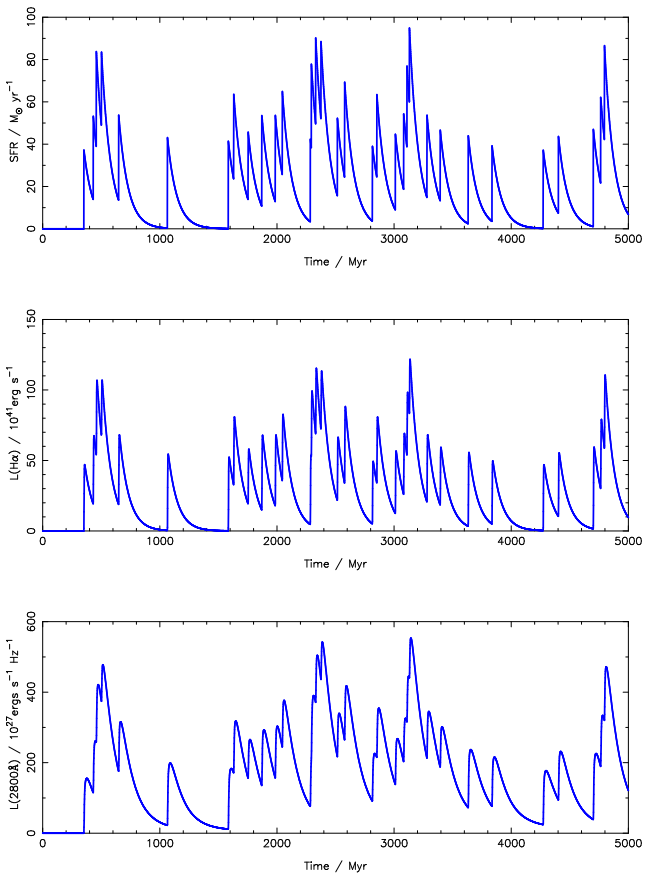

Figure 6. The star-formation rate, luminosity history in Hα and UV (2800Å) typical of our best fit models. This is for the case of exponential bursts of variable mass, with a continuous star-formation component, *i.e.* the model shown in the lower 3 panels in Figure 5. It can be seen that for long inter-burst periods galaxies are indeed quiescent in Hα, but not the UV.

of galaxies undergoing bursts will approximate continuous star-formation and results in one less free parameter. For our further analysis we confine ourselves to the BC96 models (Solar metallicity, 'kl96' atmospheres) and the Salpeter IMF (as the latter gives better results for fitting the star-formation histories, colours and mass/light ratios of galaxies, see for example Kennicutt (1983) Madau *et al.* 1998, Calzetti 1997, Lilly *et al.* 1996). We correct all (Hα, UV) points using the $A_V = 0.6$ mags Milky Way law derived in Section 5; the effect of adopting the Calzetti law is just a simple scaling to globally 3× higher star-formation rates and does not affect the details of the analysis.

To start with we modeled a simple continuous star-formation model to check our code was giving sensible results. To make it more realistic we introduced a scatter, C_σ, between galaxies following a normal distribution (slightly corrected to avoid negative star-formation rates).

The best fit results are shown in Figure 5 as a likelihood contour plot overlayed on the model points. For comparison we also show a simulated set of data points drawn from the model distribution. It can be seen that some scatter is introduced; this originates physically from the time variation of UV light even for constant star-formation. The best fit parameter values are shown in Table 4 — the model is a very bad fit to the distribution of data.

One might ask if the scatter could be explained by variation in extinction between galaxies. While it is possible this can explain some of the variation it can not explain the points with large amounts of UV emission and small amounts of Hα emission. This is because dust quenches the UV much more than the Hα — precisely the opposite effect to that sought. We next explored the effects of starbursts to see if these could plausibly explain the observed distribution.

Initially we tried fixed-mass bursts, then we tried a scheme for allowing the burst masses to vary. Since we could find little information in the literature as to an appropriate mass function to adopt for bursts we invented our own simple phenomenological scheme: bursts are parameterised by a mean mass (M_μ) and standard deviation (M_σ). The distribution is assumed to be normal. While this has no physical basis it only has 2 parameters and at least allows us to investigate the effects of mass distributions. M_μ and our global star-formation rate normalisation fixes the mean interval between bursts. Finally we have F, the fraction of the star-formation occurring in bursts. For the form of the bursts we consider two cases (modeled after BC96): a constant burst of length τ and exponential bursts of e-folding time τ.

The results of this exercise is shown in Table 4. It can be seen that the burst models provide much better fits than the the continuous models. The Monte-Carlo realisations show that the latter generate data sets like the observed one only about 1% of the time. This is because the continuous star-formation can not generate enough variation in the UV/Hα ratio. The burst models are much better and generate synthetic points which look like the data ∼ 10–20% of the time. This is because the variation in the star-formation rate is the principle cause of variation in the UV/Hα ratio. Allowing the burst mass to vary improves the fit only slightly, we conclude that our data does not constrain the shape of the burst mass function significantly. The best fit burst fraction is $\simeq 1$, indicating the burst mode is preferred. The results are illustrated graphically in the lower two rows of Figure 5 which compares the dust-corrected observational data with model realisations for a sample of key models. The likelihood contours of the main parameters are also shown.

The best fit mass of a typical burst is 2–5×10^9 $M_\odot$, corresponding to a time interval between bursts of typically ∼ 200–300 Myr and the characteristic time τ is of ∼ 100–200 Myr. This mean the bursts usually overlap in time. These values are similar to what one might expect intuitively based on the data: the chance of catching a galaxy in the Hα quiescent stage has to be of order 1/3 to reproduce the fraction of points seen with UV but no Hα.

We note that this kind of 'continuous but episodic' star-formation with several bursts per Gyr is of the same form as that found in local starburst galaxies by Calzetti (1997). Our average star-formation rates are of the same order too. In between bursts the star-formation rate and Hα flux does indeed drop close to zero while the UV persists (see Figure 6 which shows a sample time-dependence) due to the stellar lifetime effects mentioned in Section 4. Thus the zero Hα points in our data (given the error bars) are naturally explained.

Finally with these tools we were able to test how well

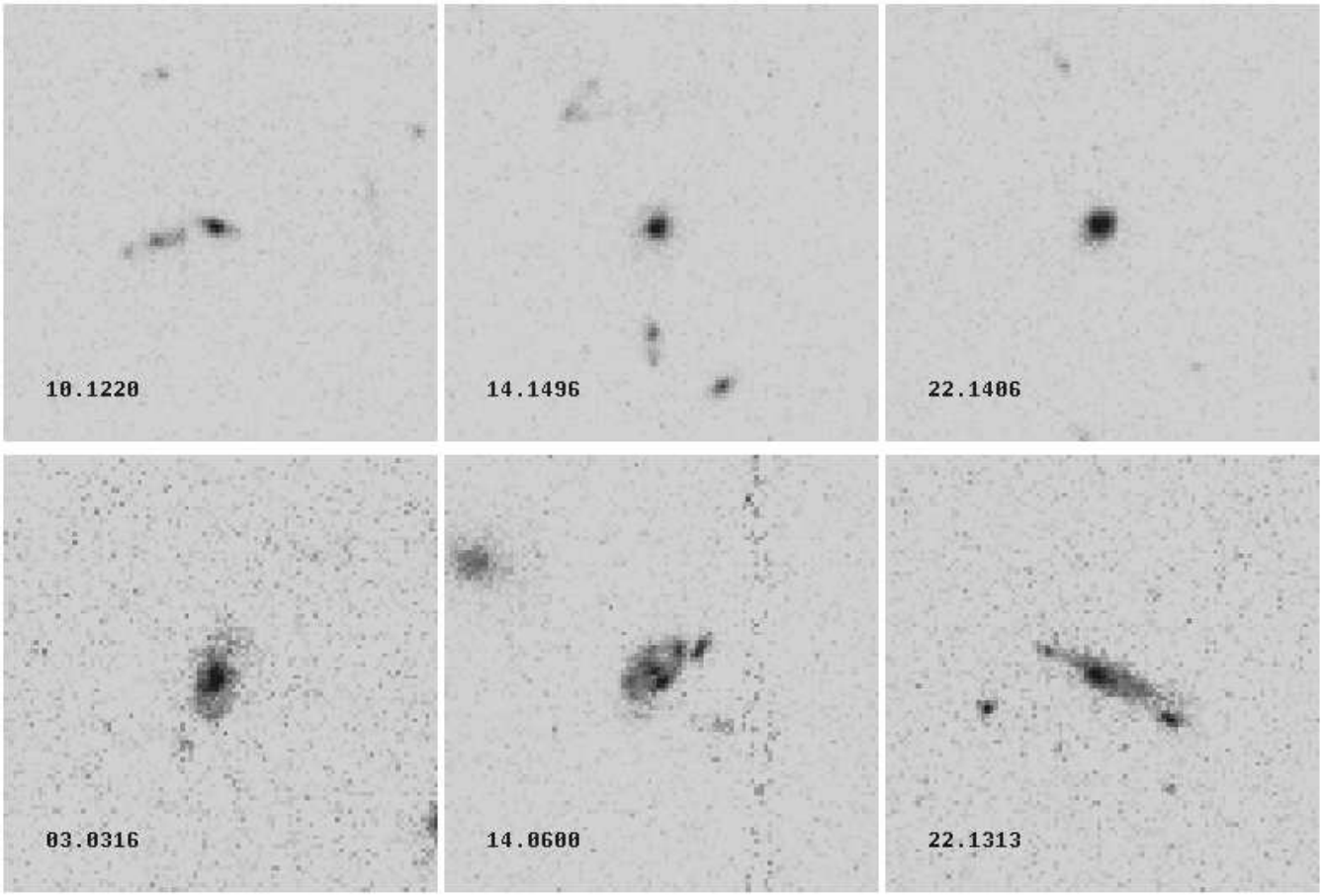

Figure 7. Postage stamps (10.1 × 10.1 arcsec) of the six galaxies having images from our HST morphology programme.

an ensemble of galaxies converged to approximating a continuous star-formation rate, as assumed in Section 5. To do this we re-ran the likelihood fitting, this time fitting for the total star-formation rate as a free parameter. The results of this gave rates of between 19 and 23 $M_{\odot}$ yr^{-1} per galaxy, which agrees well with the value of 20 $M_{\odot}$ yr^{-1} calculated in Section 5 for the same Salpeter IMF.

While these simple models could do with some elaboration to obtain a better fit, we are near the limit of what can be inferred from 13 data points. It is clear this sort of detailed approach will benefit greatly from future observations and much larger samples.

7 MORPHOLOGICAL TRENDS

Six of the galaxies in our sample have morphological information from our programme of *Hubble Space Telescope* high-resolution imaging of CFRS and LDSS2 high-redshift galaxies (Brinchmann *et al.*1998, Lilly *et al.*, 1998). This is obviously an even more limited sample, but we can look qualitatively at the dependence of star-formation rate on galaxy type.

The classifications are listed in Table 1 and postage stamps of the galaxies are shown in Figure 7. There are 3 galaxies classified as 'Peculiar'. All have detected Hα emission and blue colours ($(V-I)_{AB} < 1$) and one (14.0600) has the highest star-formation rate in our sample. Two of these are classed as 'mergers' and one as a close pair indicating an association between star-formation and interaction. There are two galaxies classed as 'Compact'. Both of these are also blue ($(V-I)_{AB} < 1.2$) and it is interesting to note that while one has quiescent Hα and strong UV the other has a large Hα excess (3.2). Finally we have 03.0316 a red spiral ($(V-I)_{AB} = 2.9$) which is quiescent in both UV and Hα.

Finally we note that galaxies with star-formation, whether inferred through Hα or UV, have the bluest $V-I$ colours ($(V-I)_{AB} < 1.2$). This is not in contradiction with the modest extinction values derived in Section 5 — an extinction of $A_V = 0.6$ mags would only redden the observed $V-I$ (rest 2800Å − B) by a small 0.4 mags whereas the difference between and old and young stellar population is of order 2–3 mags.

8 COMPARISON WITH OTHER RESULTS

There are now enough measurements of Balmer line star-formation rates at high and low redshift to construct the

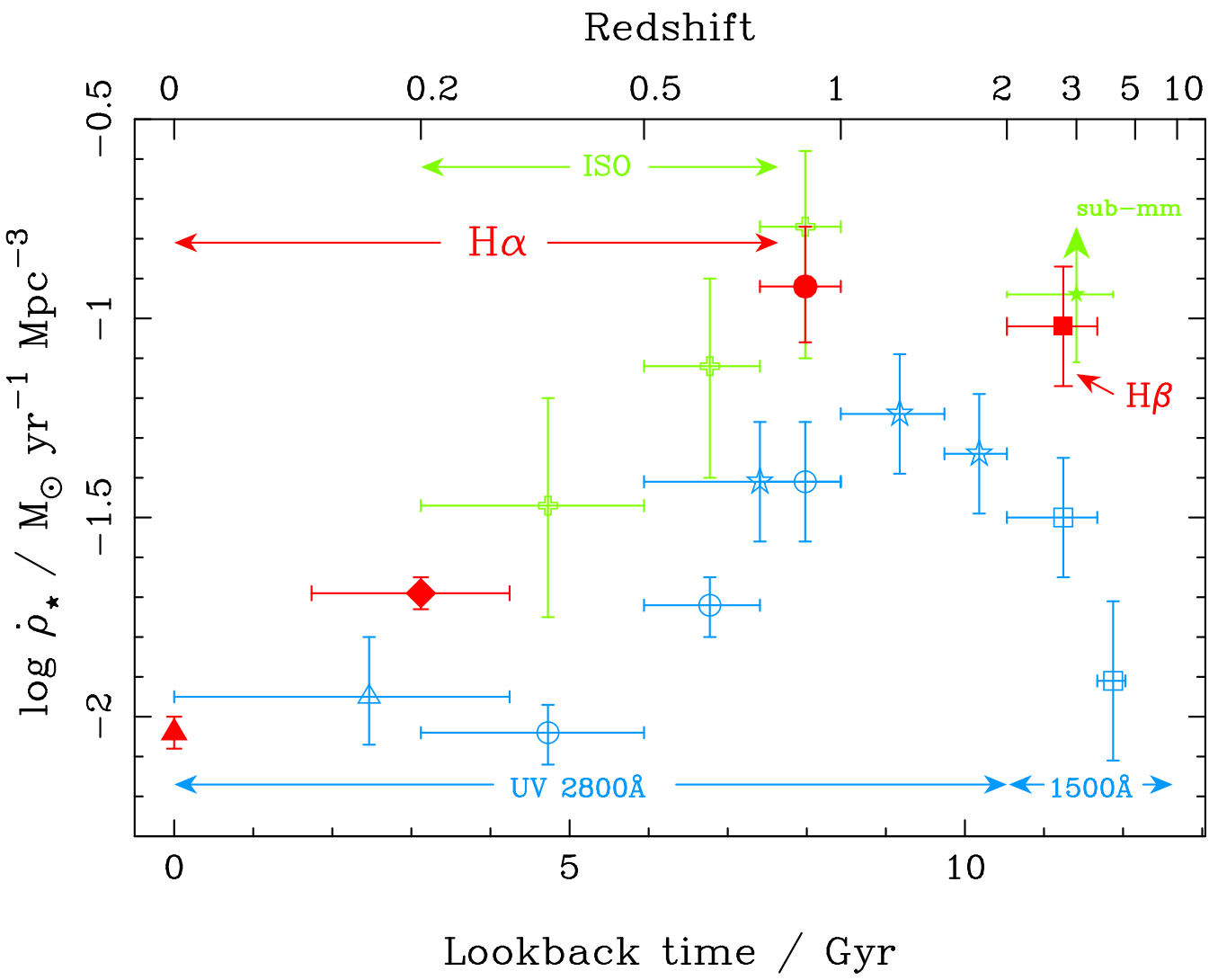

Figure 8. Star-formation history of the Universe inferred from Balmer lines (Hα and Hβ) compared to UV and far-IR/sub-mm determinations. The UV points are: Treyer *et al.* (1998; open triangle), Lilly *et al.* (1996; open circles), Connolly *et al.* (1997; open stars), Madau *et al.* (1996, 1998; open squares). The Balmer points are Gallego *et al.* (1995; filled triangle), Tresse & Maddox (1998; filled diamond), this work (filled circle), Pettini *et al.* (1998) correction of the UV Madau *et al.* point at $z = 2.8$ (filled square). We also plot the sub-mm derived point of Hughes *et al.* 1998 (solid star) and the far-IR ISO derived points of Flores *et al.* (1998) (open cross).

first star-formation history of the Universe in Balmer light to compare with the previous UV measurements. For consistency we use the Salpeter IMF, $H_0 = 50$ km s^{-1} Mpc^{-1}, $q_0 = 0.5$ throughout. All points are re-derived from their original luminosity densities in a consistent manner using the UV, Hα factors in Table 3 for BC96 (kl96) with Solar metallicity.

This is shown in Figure 8. The point at $z = 0$ comes from the Gallego *et al.* (1995) local objective prism survey and is based on Hα. Tresse and Maddox (1998) have measured the Hα luminosity function at $z = 0.2$ from the CFRS, at which point Hα is still available in the optical CFRS spectra. They find a value a factor of two higher than the UV measurements.

Our Hα measurements are used to derive a new value for the star-formation rate density in the CFRS at $z = 1$. This is higher by a factor of 3.1× than the UV point. At $z = 2.8$ we show the point derived from the work of Pettini *et al.*, who used CGS4 to measure the Hβ line in 5 of Steidel *et al.*'s galaxies. They infer star-formation rates 0.7-7 times higher than derived from the UV at 1500Å rest and typical extinctions $A(1500\text{Å}) = 1$–2 mags. We show this as a factor of 3 above the UV point. As well as the Balmer lines we also plot the point of Hughes *et al.* based on sub-mm observations and the points of Flores *et al.* (1998) from far-infrared ISO observations. It should be noted though that the derivation of the latter are qualitatively different from the Balmer line and UV measurements: the far-IR and sub-mm bands measure UV reprocessed by dust into thermal radiation and hence they are sensitive to galaxies which might not appear at all in the optical. Moreover the Hughes *et al.* points are based on an *assumed* redshift distributions for sources which have not yet been verified and has been disputed (Richards 1999). Finally it is also worth noting that the Hughes *et al.*, Connolly *et al.* and Madau *et al.* points are all based on the

same patch of sky, the Hubble Deep Field North (Williams *et al.* 1996), which may not be representative.

It can be however seen that the general trend is for the Balmer line and ISO/sub-mm measurements to find values several times higher than the UV continuum at all redshifts. The rise to $z = 1$ is preserved, arguably the fall off at $z > 2$ is preserved though given the random errors and the systematics in the dust correction no change for $z > 1$ would also be consistent with the data. Whether star-formation peaks at intermediate redshift ($z = 1$–2) or continues to high redshifts ($z > 4$) is an important test of heirarchical formation scenarios (e.g. Baugh *et al.* 1998). From the current data the question must remain open.

The agreement between the far-IR/sub-mm measurements and Balmer measurements is particularly impressive since both attempt to compensate for dust in different ways. Flores *et al.* find an upward dust correction of 2.9 ± 1.3 at $z = 1$ and extinctions of $A_V = 0.5$–0.9 mags, both consistent with our best estimates. It should be noted that independent ISO observations of the Hubble Deep Field North by Rowan-Robinson *et al.* (1997) give a conflicting value several times higher than Flores *et al.*; however the latter is derived from a 19× larger area of sky and so is probably better determined.

An important point is that the dust corrections are not many times *larger* than we have found. Larger corrections (e.g. ×15) have been argued for by authors such as Meurer *et al.* (1997) based on amounts of obscuration in powerful starburst galaxies locally. However it is not clear that the local massive starburst galaxies (e.g. Arp 220) are the right analogs of the higher redshift field galaxies. When lower luminosity starburst galaxies are studied locally they prove much less obscured (e.g. Buat & Burgarella 1998), these systems are comparable in extinction to local spirals and the sample studied here. We note though if we use the dust correction from the Calzetti law the Hα point at $z = 1$ moves up still further to 9× above the UV point. This is because if our galaxies are similar to those studied by Calzetti the HII regions suffer additional obscuration relative to the stellar continuum. This higher value would then agree with the ISO observations of Rowan-Robinson *et al.*. However the resulting high star-formation rates may be problematic in that the stellar density produced in the local universe might be too high (Madau *et al.* 1998).

9 CONCLUSIONS

From a sample of 13 galaxies observed with CGS4 we have performed the first Hα measurements of the star-formation rate at $z = 1$. We conclude the following:

(i) The Hα measurements show a star-formation rate at least three times as high as that inferred from the 2800Å continuum luminosity by Madau *et al.* (1996).

(ii) The typical dust extinction derived using standard extinction laws is only moderate ($A_V = 0.5$–1.0 mags) and very similar to that inferred in low redshift field galaxies. If there is a large population of obscured star-forming systems at $z = 1$ they are not common in known samples — their rate of occurrence in the CFRS at $z = 1$ must be $\lesssim 10\%$ or they would be detected in our data. This limit is similar to the results of Pettini *et al.* for the $z > 3$ Steidel *et al.* galaxies and consistent with deep sub-mm observations which estimate that massive obscured star-forming systems make up approximately 10% of high-redshift galaxies (Lilly *et al.* 1998B).

(iii) A cautionary note is the nature of the dust extinction law: if we follow the Calzetti attenuation prescription we imply much higher obscuration of the Hα line and a star-formation rate at $z = 1$ three times higher still. It is unclear however whether such a large correction should be applied to the integrated light of *all* galaxies at high-redshift. This issue can only be resolved by further direct measurement of the Hβ/Hα decrement in these galaxies and the derivation of the extinction to the nebular regions independent of the stellar UV flux.

(iv) The mean star-formation rate of a $z = 1$ CFRS galaxy is $\sim$ 20–60 $M_\odot$ yr^{-1} (for Salpeter IMF and the range of dust laws we have studied), which is enough to make such a L^* galaxy in a few Gyr. This is a factor of several higher than ordinary spiral galaxies of comparable luminosity today.

(v) The large scatter in the distribution of Hα to UV light is much better fit by a model in which star-formation occurs in episodic bursts with intervals of $\sim$ 0.2–0.3 Gyr and of length $\sim$ 0.1–0.2 Gyr. Pure continuous star-formation is strongly ruled out, even with variable extinction, as a sole explanation.

(vi) We find qualitative trends for star-forming systems to have blue colours and peculiar morphology (especially interactions).

(vii) The star-formation history of the Universe, as inferred from the Balmer lines, is qualitatively similar to that inferred from the UV but corrected upwards by factors of at least 2–3 at all redshifts. Although the overall form of a rise to $z = 1$ is preserved, a compilation of dust-insensitive data does not yet demonstrate with certainty whether there is a turnover beyond $z = 1$.

Finally, it is clear that the era of detailed spectral studies of high-redshift galaxies is upon us, made possible by the advent of intermediate to high-resolution spectrographs on 4m telescopes. In the next few years with larger samples and better near-IR spectrographs on 8 m class telescopes (many with the ability to spatially resolve spectra in 2D) it will be possible to model the spectral evolution of the high-redshift galaxy population in much greater details. In particular the field will be able to focus much more on detailed astrophysics (stellar/dust/gas compositions, star-formation rates, dynamics, etc.) rather than simple statistics.

ACKNOWLEDGEMENTS

We are grateful to the UKIRT time assignment committee for their support of this programme and to the staff and telescope operators of the Joint Astronomy center for their support. We especially wish to thank Gillian Wright for technical and astronomical advice. The data reduction and analysis was performed primarily with computer hardware supplied by the Anglo-Australian Observatory and STARLINK. Special thanks go to Laurence Tresse and Francois Hammer of the CFRS team for making available there raw UV and [OII] data in machine-readable form. We would also like to thank Jarle Brinchmann and Richard Ellis for providing the

HST images to allow us to explore the role of morphology. The interpretation of the data presented here was greatly aided by helpful discussions with many colleagues, especially Bob Abraham, Joss Bland-Hawthorn, Daniela Calzetti, Carlos Frenk, Claus Leitherer and Max Pettini. The authors would also like to thank an anonymous questioner at the 1997 IAU meeting in Kyoto who prompted the authors into looking in to the detailed modeling of time-dependent Hα and UV fluxes.

REFERENCES

Abraham R. G., Ellis R. S., Fabian A. C., Tanvir N. R., Glazebrook K., 1999, MNRAS, in press (astro-ph/9807140)
Baugh C. M., Cole S., Frenk C. S., Lacey C. G., 1998, ApJ, 498, 504
Bland-Hawthorn J., Maloney, P. R., 1997, PASA, 14, 59
Bland-Hawthorn J., Maloney, P. R., 1998, ApJ, in press
Brinchmann J., Abraham R., Schade D., Tresse L., Ellis R. S., Lilly S., Le Fevre O., Glazebrook K., Hammer F., Colless M. M., Crampton D., Broadhurst T., 1998, ApJ, 499, 112
Buat V., Burgarella D., 1998, A&A, 334, 772
Bruzual A. G., Charlot S., 1993, ApJ, 405, 538
Bruzual A. G., Charlot S., 1996, documentation for BC96
Calzetti D., Kinney A. L., Storchi-Bergmann T., 1994, ApJ, 429, 582
Calzetti, D. 1997, AJ, 113, 162
Connolly A. J., Szalay A. S., Dickinson M., Subbarao M. U., Brunner R. J., 1997, ApJ, 476, L11
Ellis R. S., Colless M. M., Broadhurst T. J., Heyl J., Glazebrook K., 1996, MNRAS, 280, 235
Fall S. M., Charlot S., Pei Y. C., 1996, ApJ, 464, L43
Fioc M., Rocca-Volmerange B., 1997, A&A, 326, 950
Flores H., Hammer F., T. Thuan T., Cesarsky C., Desert F. X., Omont A., Lilly S. J., Eales S., Crampton D., Le Fevre O., 1998, ApJ, in press (astro-ph/9811202)
Gallego J., Zamorano J., Arágon-Salamanca A., Regg M., 1995, ApJ, 455, L1.
Giavalisco M., Steidel C. C., Macchetto F. D., 1996, ApJ, 470, 189
Guhathakurta P., Tyson J. A., Majewski S. R., 1990, ApJ, 357, 9
Hammer F., Crampton. D., Le Fevre O., Lilly S. J., 1995, ApJ, 455, 88
Hammer F., Flores H., Lilly S. J., Crampton D., Le Fevre O., Rola C., Mallen-Ornelas G., Schade D., Tresse L., 1997, ApJ, 481, 49
Hughes D., Serjeant S., Dunlop J., Rowan-Robinson M. , Blain A., Mann R. G., Ivison R., Peacock J., Efstathiou A., Gear W., Oliver S., Lawrence A., Longair M., Goldschmidt P., Jenness T., 1998, Nature, 394, 241
Hummer D. G., Storey P. J., 1987, MNRAS, 224, 801
Kennicutt, R. C., 1983, ApJ, 272, 54
Kennicutt, R. C., 1992, ApJ, 388, 310
Leitherer C., Ferguson H. C., Heckman T. M., Lowenthal J. D., 1995, ApJ, 454, L19
Le Fevre O., Crampton. D., Lilly S. J., Hammer F., Tresse L., 1995, ApJ, 455, 60
Lilly S. J., Le Fevre O., Crampton. D., Hammer F., Tresse L., 1995, ApJ, 455, 50
Lilly S. J., Hammer F., Le Fevre O., Crampton. D., 1995B, ApJ, 455, 75
Lilly S. J., Le Fevre O., Hammer F., Crampton D., 1996, ApJ, 460, L1
Lilly S., Schade D., Ellis R., Le Fevre O., Brinchmann J., Tresse L., Abraham R., Hammer F., Crampton D., Colless M. M., Glazebrook K., Mallen-Ornelas G., Broadhurst T. J., 1998, ApJ, 500, 75
Lilly S. J., Eales S. A., Gear W. K., Bond J. R., Dunne L., Hammer F., Le Fevre O., Crampton D., 1998B, in Proceedings of the 34th Liege International Astrophysics Colloquium "NGST: Science and Technological Challenges", (ESA), in press (astro-ph/9807261)
Lowenthal J. D., Koo D. C., Guzman R., Gallego J., Phillips A. C., Faber S. M., Vogt N. P., Illingworth G. D., Gronwall C., 1997, ApJ, 481, 673
Madau P., 1995, ApJ, 441, 18
Madau P., Ferguson H. C., Dickinson M. E., Giavalisco M., Steidel C. C., Fruchter A., 1996, MNRAS, 283, 1388
Madau P., Dickinson M. E., Pozetti L., 1998, ApJ, 498, 106
Meurer G. R., Heckman T. M., Lehnert M. D., Leitherer C., Lowenthal J., 1997, AJ, 114, 54
Pei, Y. C. 1992, ApJ, 395, 130
Pettini M., Kellogg M., Steidel C. C., Dickinson M., Adelberger K. L., Giavalisco M., 1998, ApJ, 508, 539
Richards E. A., 1999, ApJ, submitted (astro-ph/9811098)
Rowan-Robinson M., Mann R. G., Oliver S. J., Efstathiou A., Eaton N., Goldschmidt P., Mobasher B., Serjeant S. B. G., Sumner T. J. Danese L., Elbaz D., Franceschini A., Egami E., Kontizas M., Lawrence A., Mcmahon R., Norgaard-Nielsen H. U., Perez-Fournon I., Gonzalez-Serrano J. I., 1997, MNRAS, 289, 490
Salpeter E. E., 1955, ApJ, 121, 161
Scalo J. M., 1986, Fundam. Cosmic. Phys., 11, 1
Smith L. F., Biermann P., Mezger P. G., 1978, Astr. Ap., 66, 65
Steidel C. C., Giavalisco M., Pettini M., Dickinson M., Adelberger K. L., 1996, ApJ, 462, L17
Tresse L., Maddox S. J., 1998, ApJ, 495, 691
Treyer M. A., Ellis R. S., Milliard B., Donas J., Bridges T. J., 1998, MNRAS, 300, 303
Williams R. E., Blacker B., Dickinson M., Dixon W. V. D., Ferguson H. C., Fruchter A. S., Giavalisco M., Gilliland R. L., Heyer I., Katsanis R., Levay Z., Lucas R. A., Mcelroy D. B., Petro L., Postman M., Adorf H.-M., Hook R., 1996, AJ, 112, 1335
Wright G. S., 1994, Experimental Astronomy, 3, 17

Table 1.

OBSERVED SAMPLE AND FLUX MEASUREMENTS

CFRS#	Exposure (secs)	z (mags)	I_{AB} (mags)	$(V-I)_{AB}$	EW [OII] (rest Å)	$F(\mathrm{H}\alpha)$ 10^{-17}ergs cm^{-2} s^{-1})	J_C (mags)	HST Morphology
00.1579	1000	0.811	22.40	1.45	33 ± 6	0.0 ± 13.9	19.67 ± 0.13	—
03.0125	1000	0.790	22.08	2.08	19 ± 7	20.1 ± 7.8	20.19 ± 0.10	—
03.0133	1500	1.048	22.45	1.00	65 ± 16	52.9 ± 33.9	> 21.87	—
03.0316	1500	0.815	21.98	2.91	12 ± 2	0.0 ± 6.8	> 22.87	Spiral
03.0615	500	1.048	22.01	0.96	27 ± 5	0.0 ± 24.9	> 20.87	—
03.1534	2000	0.798	22.45	0.70	39 ± 8	68.9 ± 23.8	20.70 ± 0.23	—
10.1220	1200	0.909	22.36	0.97	20 ± 4	75.5 ± 16.2	> 21.69	Peculiar (merger)
14.0600	4000	1.038	21.53	0.69	27 ± 9	108.2 ± 19.0	19.08 ± 0.19	Peculiar (close pair)
14.0818	1000	0.899	21.02	1.12	19 ± 2	0.0 ± 30.5	18.74 ± 0.11	—
14.1496	2400	0.899	21.80	1.13	28 ± 6	0.0 ± 15.7	19.10 ± 0.10	Compact
22.0770	3000	0.819	21.78	1.58	39 ± 5	42.9 ± 6.4	20.74 ± 0.18	—
22.1313	6000	0.819	21.74	0.84	40 ± 5	40.5 ± 3.6	20.36 ± 0.08	Peculiar (merger)
22.1406	4000	0.818	22.16	1.16	55 ± 4	78.3 ± 6.2	21.24 ± 0.20	Compact

Table 2.

DERIVED LUMINOSITIES AND VELOCITY WIDTHS

CFRS#	$L(\mathrm{H}\alpha)$ [(i)] (10^{41}ergs s^{-1})	$L([OII])$ [(i)] (10^{41}ergs s^{-1})	$L(2800\text{Å})$ [(i)] (10^{27}ergs s^{-1} Hz^{-1})	FWHM [(ii)] rest km/sec
00.1579	0.0 ± 5.2	3.8 ± 0.5	18.5	—
03.0125	7.1 ± 2.8	6.5 ± 1.5	10.6	457
03.0133	34.7 ± 22.2	12.9 ± 1.8	52.2	392
03.0316	0.0 ± 2.5	2.4 ± 0.4	3.6	—
03.0615	0.0 ± 16.3	22.6 ± 2.4	81.3	—
03.1534	24.8 ± 8.6	13.2 ± 1.8	42.7	283
10.1220	36.2 ± 7.8	7.7 ± 1.4	43.5	260
14.0600	69.5 ± 12.2	36.4 ± 8.3	154.9	377
14.0818	0.0 ± 14.3	16.1 ± 1.9	125.3	—
14.1496	0.0 ± 7.4	14.9 ± 1.9	60.5	—
22.0770	16.3 ± 2.4	13.5 ± 1.1	29.8	unresolved
22.1313	15.4 ± 1.4	19.5 ± 2.5	70.8	251
22.1406	29.8 ± 2.4	21.8 ± 1.2	33.3	279

Notes:

(i) To correct for dust using the final extinction values derived in Section 5 multiply the above values by the following factors: $L(\mathrm{H}\alpha)$: $\times 1.6$, $L([OII])$: $\times 2.4$, $L(2800\text{Å})$: $\times 3.1$.

(ii) The instrumental resolution ranges from 70–100 km/s (FWHM) and has been subtracted in quadrature from these values.

Table 3.

CONVERSIONS OF Hα,UV TO STAR-FORMATION RATES

Luminosities are for 1 $M_\odot$ yr^{-1}.

Model	$Z/Z_\odot$	IMF	L(Hα) (10^{41}ergs s^{-1})	L(1500Å) (10^{27}ergs s^{-1} Hz^{-1})			L(2800Å) (10^{27}ergs s^{-1} Hz^{-1})			L(2800Å)/L(Hα) (10^{-14} Hz^{-1})
				0.1 Gyr	1.0 Gyr	3.0 Gyr	0.1 Gyr	1.0 Gyr	3.0 Gyr	(1 Gyr)
BC96 (kl96)	0.02	SC	0.68	4.36	**6.64**	7.19	2.84	**6.23**	8.63	9.2
BC96 (kl96)	0.20	SC	0.58	3.93	**5.36**	5.40	2.84	**5.35**	6.58	9.2
BC96 (kl96)	0.40	SC	0.50	3.80	**4.82**	4.83	2.89	**4.96**	5.80	9.9
BC96 (kl96)	1.00	SC	0.40	3.48	**4.02**	4.02	2.93	**4.36**	4.81	10.9
BC96 (kl96)	2.50	SC	0.28	3.07	**3.33**	3.33	2.93	**3.88**	4.10	13.9
BC96 (gs95)	1.00	SC	0.61	3.64	**4.39**	4.40	2.39	**3.72**	4.13	6.1
BC96 (gsHR)	1.00	SC	0.61	3.64	**4.39**	4.40	2.39	**3.72**	4.13	6.1
PEG (Pad)	1.00	SC	0.41	4.13	**4.72**	4.72	3.15	**4.80**	5.39	11.7
PEG (Gen)	1.00	SC	0.45	3.84	**4.42**	4.43	2.94	**4.57**	5.18	10.2
M98	1.00	SC			**3.50**			**5.10**		
BC96 (kl96)	0.02	SP	2.23	10.21	**12.56**	12.87	6.29	**9.48**	10.78	4.2
BC96 (kl96)	0.20	SP	1.96	9.27	**10.93**	10.96	6.32	**8.85**	9.53	4.5
BC96 (kl96)	0.40	SP	1.70	9.22	**10.49**	10.50	6.59	**8.76**	9.24	5.1
BC96 (kl96)	1.00	SP	1.35	8.61	**9.37**	9.37	6.85	**8.46**	8.73	6.3
BC96 (kl96)	2.50	SP	0.90	7.62	**7.99**	7.99	6.87	**7.94**	8.07	8.8
BC96 (gs95)	1.00	SP	1.97	8.73	**9.77**	9.77	5.50	**7.00**	7.25	3.6
BC96 (gsHR)	1.00	SP	1.97	8.73	**9.77**	9.77	5.50	**7.00**	7.25	3.6
PEG (Pad)	1.00	SP	1.19	8.64	**9.31**	9.31	6.16	**7.68**	7.97	6.5
PEG (Gen)	1.00	SP	1.28	8.02	**8.66**	8.66	5.68	**7.16**	7.46	5.6
K83	1.00	SP-like	1.12							
M96	1.00	SP			**11.06**			**7.04**		
M98	1.00	SP	1.41		**8.00**			**7.90**		

Notes:

(i) SC and SP are the Scalo (1986) and Salpeter (1955) IMFs

(ii) K83 is Kennicutt's (1983) conversion for a Salpeter-like IMF

(iii) M96 is Madau *et al.* (1996) values for 0.1-1 Gyr, derived from Bruzual & Charlot (1993); M98 are the values from Madau *et al.* (1998)

(iv) BC96 are values derived from Bruzual & Charlot (1996) models, multi-metallicity 'kl96' stellar spectra are based on stellar model atmospheres (Lejeune *et al.*, 1996, Kurucz, 1995) and 'gs95' are based on observed Gunn & Stryker (1983) spectra. All use the 'Padova' stellar evolutionary tracks.

(v) PEG are values derived from the PEGASE models (Fioc *et al.* 1997) for the 'Padova' and 'Geneva' stellar evolutionary tracks respectively.

Table 4. Best fit model parameters

Description of model	Best fit parameters with errors, in the form $P_{\rm fitted} = 2\sigma < 1\sigma <$ **best value** $< 1\sigma < 2\sigma$	$\log(L_{best})$	Monte-Carlo deviation of L_{best} (percentiles)
Continuous star-formation rate	$C_\sigma = 0.61 < 0.65 <$ **0.70** $< - < -$	−38.42	98.6
Continuous plus constant starbursts of fixed mass	$F = 0.87 < 0.90 <$ **1.00** $< - < -$ C_σ not relevant because $F_{best} = 1.0$ $M_\mu = 1.23 < 1.31 <$ **1.39** $< 1.48 < 1.57 \times 10^9\ M_\odot$ $\tau = - < 50.6 <$ **80.0** $< 88.4 < 97.8$ Myr	−36.09	87.4
Continuous plus constant starbursts of variable mass	$F = 0.93 < 0.96 <$ **1.00** $< - < -$ C_σ not relevant because $F_{best} = 1.0$ $M_\mu = 1.57 < 1.84 <$ **2.15** $< 2.56 < 3.03 \times 10^9\ M_\odot$ $M_\sigma = 0.18 < 0.22 <$ **0.30** $< 0.32 < 0.34$ $\tau = 65.9 < 72.6 <$ **80.0** $< 107.0 < 143.1$ Myr	−35.88	82.0
Continuous plus exponential starbursts of fixed mass	$F = 0.83 < 0.94 <$ **1.00** $< - < -$ C_σ not relevant because $F_{best} = 1.0$ $M_\mu = 4.28 < 4.71 <$ **5.18** $< 5.54 < 5.93 \times 10^9\ M_\odot$ $\tau = 122.7 < 140.1 <$ **160.0** $< 170.5 < 181.7$ Myr	−36.21	88.4
Continuous plus exponential starbursts of variable mass	$F = 0.92 < 0.96 <$ **1.00** $< - < -$ C_σ not relevant because $F_{best} = 1.0$ $M_\mu = 2.67 < 2.91 <$ **3.16** $< 3.37 < 3.60 \times 10^9\ M_\odot$ $M_\sigma = - < - < -$ **0.10** $< 0.13 < 0.17$ $\tau = 65.0 < 72.1 <$ **80.0** $< 106.3 < 141.4$ Myr	−36.04	88.0

Notes:

(i) Parameter ranges '1σ' and '2σ' correspond to $\Delta \log \mathcal{L} = -0.5, -1.0$.

(ii) M_σ is expressed as a fraction of M_μ.